JOURNAL OF AIRCRAFT
Vol. 41, No. 4, July–August 2004

Improved Understanding of Transonic Flutter: A Three-Parameter Flutter Surface

Denis B. Kholodar,* Earl H. Dowell,† Jeffrey P. Thomas,‡ and Kenneth C. Hall§
Duke University, Durham, North Carolina 27708

An understanding of transonic flutter is often critical for high-speed aircraft development. A presentation of the transonic flutter velocity as a function of the Mach number and mass ratio is shown here to provide many advantages. Such a presentation offers new insights when comparing computational and wind-tunnel flutter results. The benefits of such a presentation are also evident in parameter studies. Finally, the subject of flutter similarity rules for airfoils of different thicknesses is also addressed.

Nomenclature

a	=	nondimensional location of airfoil elastic axis, e/b
a_0	=	stagnation speed of sound
b, c	=	semichord and chord, respectively
e	=	location of airfoil elastic axis, measured positive aft of airfoil midchord
h	=	airfoil plunge degree of freedom (DOF)
I_α	=	second moment of inertia about elastic axis
K_h, K_α	=	airfoil plunge stiffness and torsional stiffness about elastic axis, respectively
L	=	aerodynamic lift
M	=	freestream Mach number
M_{ea}	=	aerodynamic moment about elastic axis
m	=	airfoil sectional mass
r_α	=	radius of gyration of airfoil about elastic axis; r_α^2 is identical to I_α/mb^2
S_α	=	first moment of inertia about elastic axis
U	=	freestream velocity
V	=	reduced velocity; identical to $U/\omega_\alpha b$
V_μ	=	flutter speed index; identical to $U_f/\sqrt{\mu}\omega_\alpha b$
x_α	=	airfoil static unbalance; identical to S_α/mb
α	=	airfoil pitch DOF
Δ_X	=	relative difference of two variables, X_1 and X_2; identical to $(X_1 - X_2)/X_1$
δ	=	thickness of airfoil
ε	=	frequency-dependent exponent in ψ
μ	=	mass ratio; identical to $m/\pi\rho b^2$
ρ	=	freestream density
Σ	=	compatibility surface (relates V and M)
χ	=	transonic aerodynamic similarity parameter
ψ	=	transonic flutter similarity parameter
$\omega, \bar{\omega}$	=	frequency and reduced frequency based on airfoil chord; $\bar{\omega}$ is identical to $\omega c/U$
ω_α, ω_h	=	uncoupled natural frequencies of pitch and plunge DOF
ω_1, ω_2	=	coupled structural natural frequencies

Received 13 January 2003; revision received 23 July 2003; accepted for publication 8 August 2003.

*Research Associate, Department of Mechanical Engineering; currently Research Associate, Department of Aeronautics, U.S. Air Force Academy, Colorado Springs, Co 80840. Member AIAA.

†J. A. Jones Professor, Department of Mechanical Engineering and Materials Science, Director, Center for Nonlinear and Complex Systems, and Dean Emeritus, School of Engineering. Fellow AIAA.

‡Research Assistant Professor, Department of Mechanical Engineering and Materials Science. Member AIAA.

§Professor and Chairman, Department of Mechanical Engineering and Materials Science. Associate Fellow AIAA.

Introduction

BENDIKSEN[1] has made several interesting and important observations about transonic flutter boundaries as determined in a typical transonic wind-tunnel test. In particular he has noted that single-DOF flutter may occur at low values of air density or dynamic pressure when the test is conducted at a fixed Mach number by increasing the wind-tunnel stagnation pressure and, therefore, air static density and dynamic pressure. The present authors have conducted an initial parameter study[2] in transonic range for a two-DOF airfoil in plunge and pitch using the methods from this paper and that work is extended here to further consider Bendiksen's observations as well as other physical parameters not explored in Ref. 2.

Bendiksen's results are reconfirmed and the needs for careful identification of the flutter boundary in the transonic range and for extensive data sets to define such boundaries are emphasized. Fortunately, newly emerging methods that provide much more efficient calculation of transonic flutter boundaries are now becoming available.[2–4] Also, the results of Bendiksen and the present results suggest the need to reconsider how transonic wind-tunnel flutter tests are conducted. For example, it may be desirable to fix stagnation pressure and vary Mach number rather than vice versa to determine the experimental flutter boundary when testing in the transonic flutter regime.

Governing Equations and Computational Method

Consider a typical two-DOF airfoil section with the equations of motion

$$m\ddot{h} + S_\alpha\ddot{\alpha} + K_h h = -L, \qquad S_\alpha\ddot{h} + I_\alpha\ddot{\alpha} + K_\alpha\alpha = M_{\text{ea}} \quad (1)$$

The left-hand-side terms represent a linear structural model approximation for the plunge and pitch coordinates. The right-hand-side terms represent the aerodynamic loading terms, which for this study are based on the harmonic balance approach applied to a discrete computational fluid dynamic (CFD) model of the inviscid Euler equations. A summary of the method, its application to parametric flutter analysis, and convergence study are given in a recent work.[2] For a more detailed description of the inviscid CFD harmonic balance aerodynamic Euler-based method see Ref. 5.

Flutter Boundary Surface

Computational results were initially obtained for a NACA 65A004 airfoil and 18 Mach numbers ($0.3 \le M \le 1.0$) in the reduced frequency range $0.0 \le \bar{\omega} \le 0.8$. The three-dimensional parameter (V_f, M, μ) surface for the flutter is shown in Fig. 1a for a mass ratio range $20 \le \mu \le 200$.

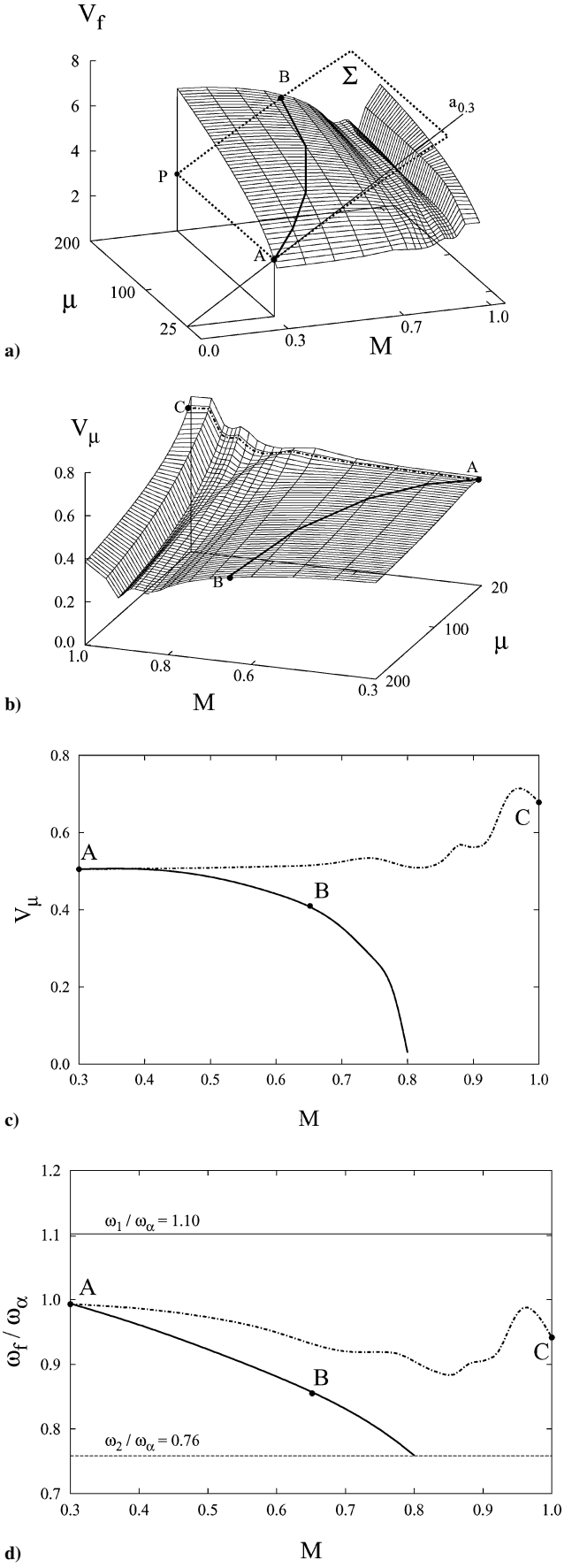

Fig. 1 NACA 65A004 computational results: a) flutter speed surface vs Mach number and Mass ratio, b) flutter speed index surface vs Mach number and mass ratio, c) flutter speed index vs Mach number, and d) flutter frequency vs Mach number (NACA 65A004, $\omega_h/\omega_\alpha = 0.8$, $x_\alpha = 0.25$, $r_\alpha^2 = 0.75$, $a = -0.6$).

A possible flight-test flutter trajectory is denoted by the line AB. In constructing the flight flutter boundary, the authors have (for a given Mach number) used the three-parameter flutter surface to ensure that the mass ratio and flight flutter speed index are compatible for a given Mach number and altitude. Thus, in the language of the flutter engineer, we have ensured that the mass ratio, flutter speed index, and Mach number of the flight flutter boundary correspond to matched or compatible points in the three-parameter surface for the flutter boundary. Suppose the airfoil flutters at point A, where the Mach number is $M = 0.3$ and the mass ratio is $\mu = 25$. Now consider the compatibility relationship between the reduced velocity, V, and Mach number, M:

$$V \equiv U(1/\omega_\alpha b) = M\sqrt{(T/T_0)}(a_0/\omega_\alpha b) \tag{2}$$

Equation (2) defines the ratio $a_0/\omega_\alpha b$ at point A, which is denoted by the $a_{0.3}$ line in Fig. 1a for the given Mach number (i.e., $M = 0.3$). Note, however, that if the absolute temperature ratio $\sqrt{T/T_0}$ changes as the Mach number is increased, the compatibility surface Σ will not be a plane. The compatibility surface Σ was computed for values $\sqrt{T/T_0}$ taken from tables of compressible-flow functions of isentropic perfect gas. The curve AB is the intersection of the compatibility surface Σ with the flutter surface V_f.

A gain of the altitude during a flight will cause the mass ratio to grow from its value at A to that at point P. Now to reach the flutter condition at this altitude, the pilot would have to increase the Mach number from $M = 0.3$ (point P) to $M = 0.65$ (point B).

In the literature the flutter boundary is often represented by the flutter speed index (the ratio of the nondimensional flutter speed and the square root of mass ratio), which here will be denoted by V_μ. In the following, for the three-dimensional parameter flutter surfaces, the Mach number axis is often pointed in the left direction to provide a better view of the transonic dip region.

A flutter speed index surface corresponding to Fig. 1a is shown in Fig. 1b. In addition to the considered possible flight-test trajectory AB, Fig. 1b shows the flutter trajectory AC originating from point A. AC corresponds to a constant mass ratio path on the flutter surface. These two trajectories, when projected on V_μ vs M plane as in Fig. 1c, appear dramatically different from each other. For the considered example of a flight-test curve, the intersection of the flutter and Σ surfaces beyond point B occurs with little increase in Mach number (and therefore flutter velocity), while the mass ratio keeps growing steadily. Near $M = 0.8$ the trajectory becomes nearly parallel with the μ axis, thus causing V_μ in Fig. 1c to go rapidly to zero. (At $M = 0.8$ the calculated mass ratio is $\mu \approx 45{,}000$.) The flutter frequency at that point is essentially the same as the coupled in vacuo natural frequency corresponding to a dominant plunge motion (i.e., $\omega_1/\omega_\alpha = 0.76$; see Fig. 1d). Correspondingly, the flutter eigenvector (not shown here) is dominated by the plunge motion. This is an example of single-DOF flutter, but note that the critical aeroelastic mode is a mass coupled natural mode, albeit one that is plunge dominated.

An example wherein AB is a possible wind-tunnel flutter trajectory is considered next.

Comparison of Wind-Tunnel and Computational Results

Reference 6 provides detailed data from a NACA 0012 Benchmark Model wind-tunnel experiment performed in the NASA Langley Transonic Dynamics Tunnel. The flutter trajectory for the values of the speed of sound from Ref. 6 is marked on the computed flutter surface (see Fig. 2a). The trajectory has a gap in the Mach number range $0.82 < M < 0.92$, where the compatibility surface (not shown here, described in the previous section) passes above the transonic dip valley.

Because the flutter velocity per se (or Mach number) is taken to be identical for both the computational and experimental models, it is advantageous for comparison of the computational and experimental results to consider $1/\mu_f$ instead of the flutter speed index $V_\mu \equiv V_f/\sqrt{\mu}$. A plot of $1/\mu_f$ vs the Mach number is discussed next

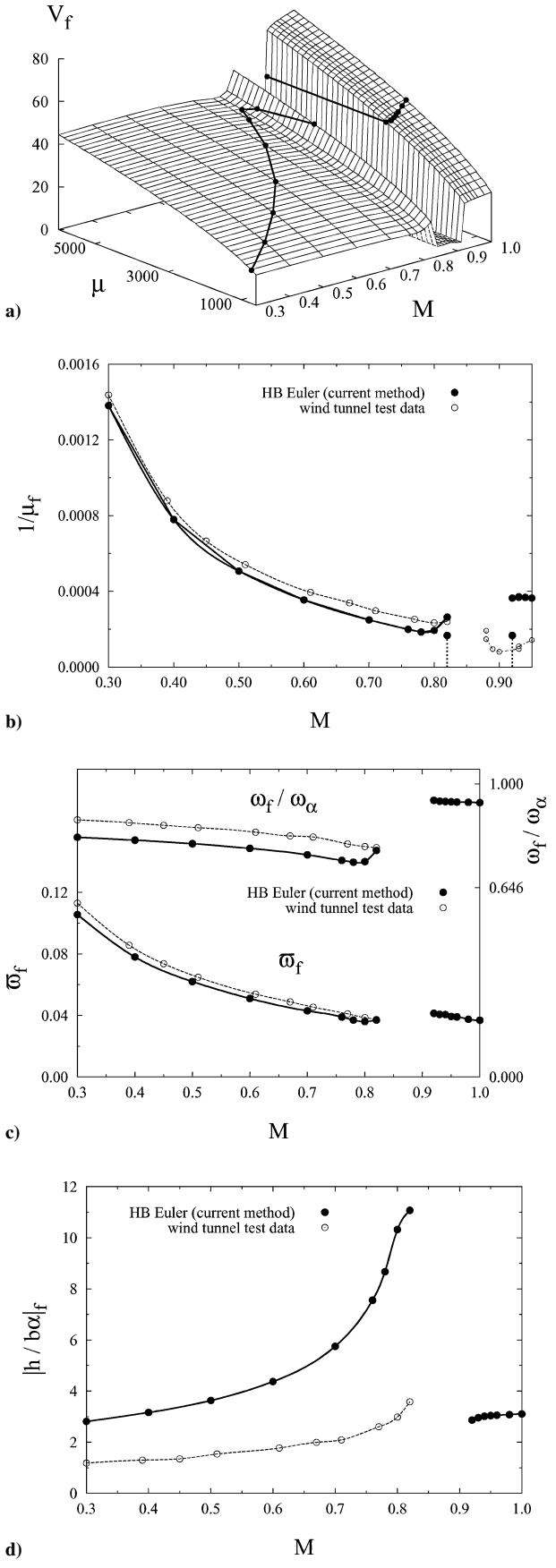

Fig. 2 Comparison of computational results with those from wind-tunnel testing: a) flutter speed surface vs Mach number and mass ratio with the numerically simulated wind-tunnel trajectory as indicated, b) inverse flutter mass ratio vs mach number, c) flutter-reduced frequency and frequency vs mach number, and d) flutter mode vs mach number (NACA 0012, $\omega_h/\omega_\alpha = 0.646$, $x_\alpha = 0$, $r_\alpha^2 = 1.024$, $a = 0$).

(see Fig. 2b). Note that the experimental pitch and plunge apparatus has a rather heavy mass of 192 lb for a 32×16 in.^{2} wing.

In the range $0.30 \leq M \leq 0.82$, there is good agreement between the numerical and experimental results.

In the range $0.82 < M < 0.88$, no (experimental) flutter data were presented in Ref. 6. As has already been mentioned, results of the Euler harmonic balance (HB) method reveal that in the range $0.82 < M < 0.92$ there is no theoretical flutter boundary for the considered values of the mass ratio and speed of sound. The dotted lines (at $M = 0.82$ and 0.92) that go down to low values of $1/\mu_f$ are the expected results for values of μ beyond those considered in the numerical study. It is also possible that at very high mass ratios the value of V_f in the transonic dip valley region (Fig. 2a) could rise enough to intersect with the compatibility surface in that Mach number range, making the dotted lines in Fig. 2b connect at very low values of $1/\mu_f$.

In the range $0.88 \leq M \leq 0.95$, Rivera and his colleagues[6] observed a "plunge instability," where "the flutter motion consisted of primarily the plunge mode." The Euler HB method branch in this range of Mach number starts at higher Mach numbers and the $1/\mu_f$ values are larger than those of the experiment. The reason for these disagreements between experiment and theory is believed to be the influence of viscous effects (which are not accounted for in Euler aerodynamic models): "Flow Visualization using tufts indicated strong shock-induced separation for this Mach number range."[6] Moreover, viscosity increases the effective airfoil thickness as perceived by the flow. Increased thickness causes a shift of the transonic dip to lower Mach numbers and also, for a given mass ratio, lowers the flutter velocity at Mach numbers above the transonic dip. The effect of airfoil thickness per se on flutter is studied in the next section.

In the $0.30 \leq M \leq 0.82$ range, frequency and reduced frequency of flutter results correlate well between the computational and wind-tunnel models (see Fig. 2c). (No experimental flutter frequency or mode data were recorded for high transonic Mach numbers in Ref. 6.) The flutter frequency results show that this is a coalescence flutter with a dominating plunge mode. This is also seen in Fig. 2d, where the flutter eigenvector is shown.

Aerodynamic and Aeroelastic Similarity

Using the full potential equation, Bendiksen[7] derived similarity parameters for unsteady transonic flows. These similarity parameters allow a comparison of equivalent flows over airfoils of the same families but with different thicknesses and operating at different Mach numbers. One basic aerodynamic similarity variable is[7]

$$\chi = \frac{1 - M^2}{[(\gamma + 1)M^2\delta]^{\frac{2}{3}}} \tag{3}$$

Bendiksen noted that χ (obtained in the limit of steady flow) differs slightly from the classical von Karman result, but χ is the same similarity parameter as that obtained by Spreiter[8,9] by fitting experimental data.

The other similarity parameter used here to test aeroelastic similarity rules for prediction of a flutter boundary shift with different airfoil thicknesses is the transonic flutter similarity parameter[7]:

$$\psi = V_\mu^2/\pi[(\gamma + 1)M^2]^{\frac{1}{3}}\delta^{\frac{1}{3}-\varepsilon(\bar{\omega})} \tag{4}$$

"The form and magnitude of the exponent $\varepsilon(\bar{\omega})$ can be established analytically, by numerical (CFD) calculations, or deduced from wind tunnel tests on aeroelastic models," wrote Bendiksen.[7] Here Eqs. (3) and (4) are applied to NACA 0004 and NACA 0012 airfoils.

The flutter speed index surfaces for both NACA 0004 and NACA 0012 airfoils are shown in Figs. 3a and 3b. As expected, for the thicker airfoil the transonic dip occurs at the lower Mach numbers.

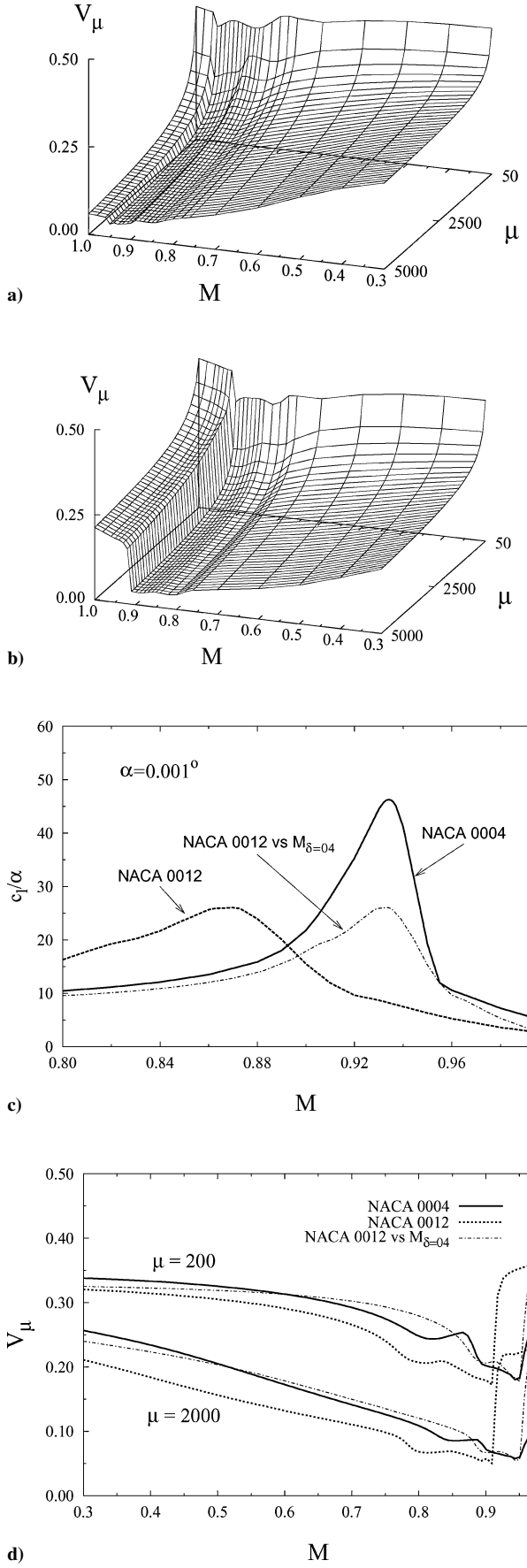

Fig. 3 NACA 0004 and 0012 airfoils aerodynamic and aeroelastic similarity results: a) NACA 0004 and b) NACA 0012 airfoil flutter speed index vs Mach number and mass ratio; c) ratio of steady lift to pitch angle vs Mach number and d) flutter speed index ($\omega_h/\omega_\alpha = 0.8$, $x_\alpha = 0.25$, $r_\alpha^2 = 0.75$, $a = 0$).

From Eq. (3) the aerodynamically similar Mach numbers for these airfoils satisfy the relationship

$$\frac{1 - M_{12}^2}{1 - M_{04}^2}\left(\frac{M_{04}}{M_{12}}\right)^{\frac{4}{3}} = 3^{\frac{2}{3}} \tag{5}$$

where the subscript indicates the airfoil thickness-to-chord percent ratio. Figure 3c shows the lift slope coefficient as a function of Mach number. This figure shows that the lift slope coefficient peaks align for aerodynamically similar Mach numbers.

The difference in the flutter speed index for $\mu = 200$ and 2000 is shown in Fig. 3d. From these results one can conclude that, due to the alignment of the lift slope coefficients, the transonic dips also become aligned for aerodynamically similar Mach numbers.

The next step is to test the aeroelastic similarity rule, Eq. (4). This is done in Fig. 4a, where the transonic flutter similarity parameter is shown vs aerodynamically similar Mach number [for the case of $\varepsilon(\bar{\omega}) = 0$]. In the transonic range of Mach numbers, the flutter similarity parameters for these two airfoils are close until the Mach numbers reach $M_{\delta=04} \approx 0.95$ at the end of the transonic dip. Flutter-reduced frequencies, amplitude ratios, and phases are shown in Figs. 4b, 4c, and 4d respectively. With the exception of the flutter-reduced frequency and eigenmode for Mach numbers above the transonic dip, the equivalent similarity quantities in Figs. 4b–4d agree well.

Structural–Inertial and Geometrical Parameter Sensitivity

In functional form and to emphasize the parameters involved, the aeroelastic equations can be written as

$$[\boldsymbol{F}(a, x_\alpha, r_\alpha, \text{ geom}, M, \bar{\omega}, \mu, (\omega_h/\omega_\alpha, V)] \begin{Bmatrix} h/b \\ \alpha \end{Bmatrix} = \mathbf{0}$$

In the following several sections, the effects of these parameters on the flutter speed index are briefly studied.

Static Unbalance Effect

Dependence of the flutter speed index on the airfoil static unbalance, $x_\alpha \equiv S_\alpha/mb = x_{cg}/b$ is shown in Fig. 5.

When the elastic axis is behind or coincides with the center of gravity, x_{cg}, (i.e., $x_\alpha \leq 0$), for Mach numbers up to $M = 0.88$, the flutter occurs at very low reduced frequencies $0.01 \leq \bar{\omega} \leq 0.05$ and the flutter speed index is very high (see Fig. 5a). As the Mach number exceeds $M \geq 0.89$ the reduced frequency of flutter rises to values of $0.35 \leq \bar{\omega} \leq 0.55$ and the flutter speed index drops to the values below 1. For Mach numbers $M \geq 0.95$, the computations showed no flutter boundary for low mass ratios.

For small positive values of x_α (e.g., $x_\alpha = 0.10$), it is observed that in the vicinity of $M \sim 0.89$ there is a jump in the flutter speed index. As in the case of a negative or zero x_α, for $x_\alpha = 0.10$ for $M \geq 0.95$, the computations showed no flutter boundary for low mass ratios. For $x_\alpha \geq 0.25$ the flutter speed index remains below 1 in the range of Mach numbers considered here. Note that the transonic dip becomes more evident as x_α grows from 0.25 to 1.00.

Radius of Gyration Effect

Dependence of the flutter speed index on the radius of gyration of airfoil about the elastic axis, $r_\alpha^2 \equiv I_\alpha/mb^2$, is shown in Fig. 6. These results show that an increase in the radius of gyration tends to increase the flutter speed index, especially for higher mass ratios. A similar conclusion was reached for different airfoil geometries (results not shown).

Mass Ratio and Ratio of Uncoupled Natural Frequencies Effect

All the flutter velocity results presented in this paper show a relatively weak dependence on the mass ratio per se, and as μ is increased the flutter speed index is generally decreasing.

Dependence of the flutter speed index on the bending-torsion frequency ratio, ω_h/ω_α, is shown in Fig. 7.

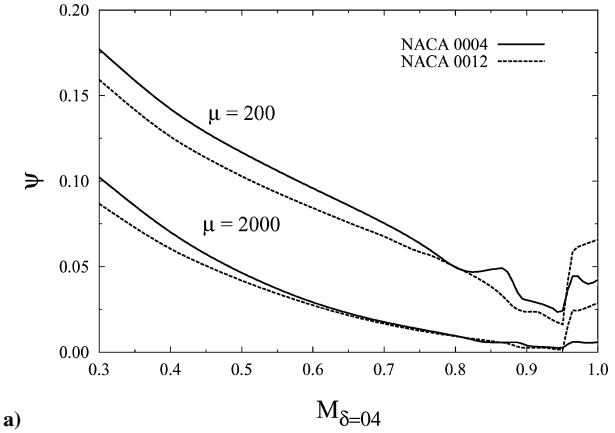

a)

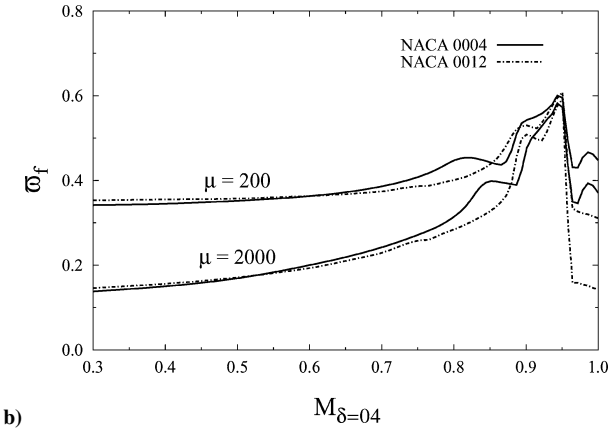

b)

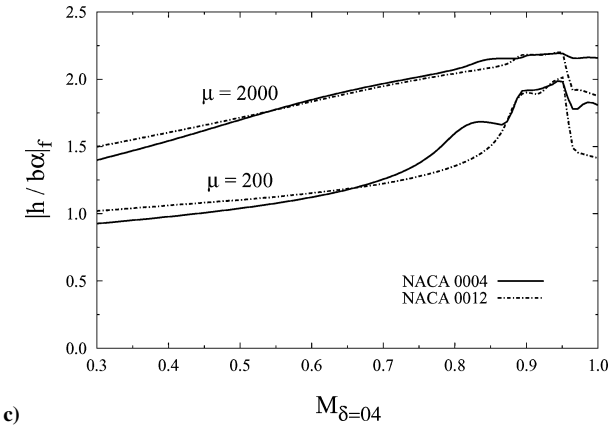

c)

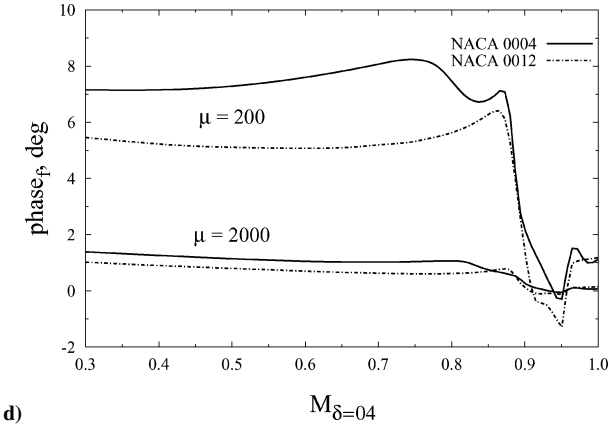

d)

Fig. 4 NACA 0004 and 0012 airfoils flutter similarity results: a) transonic similarity parameter, b) reduced frequency, c) amplitude ratio, and d) Phase. All plotted vs Mach number that corresponds to NACA 0004 airfoil ($\omega_h/\omega_\alpha = 0.8$, $x_\alpha = 0.25$, $r_\alpha^2 = 0.75$, $a = 0$).

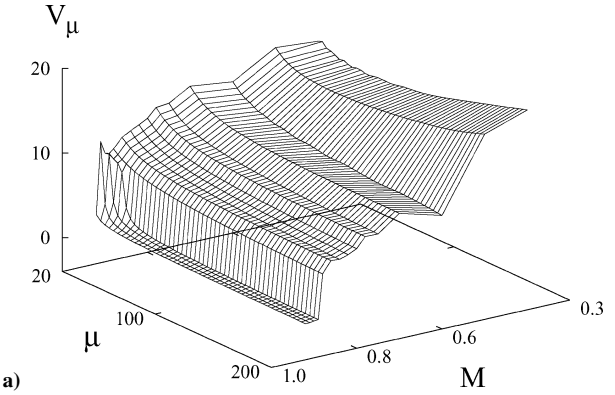

a)

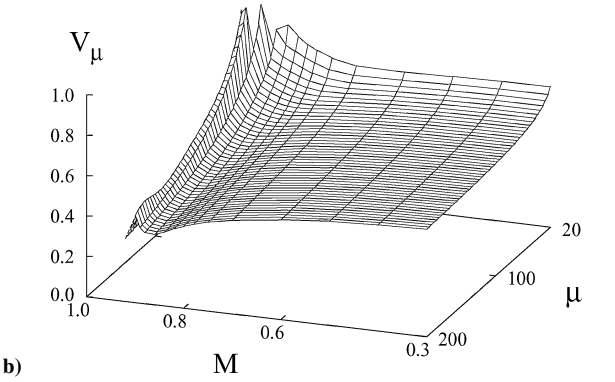

b)

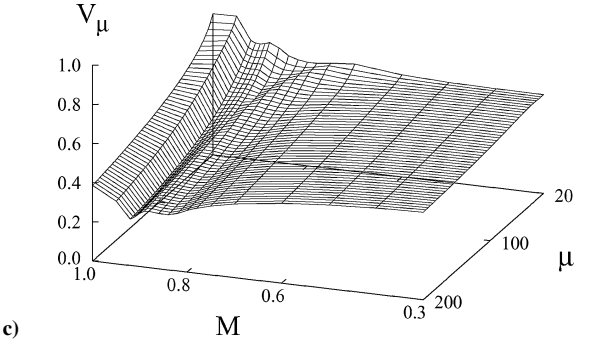

c)

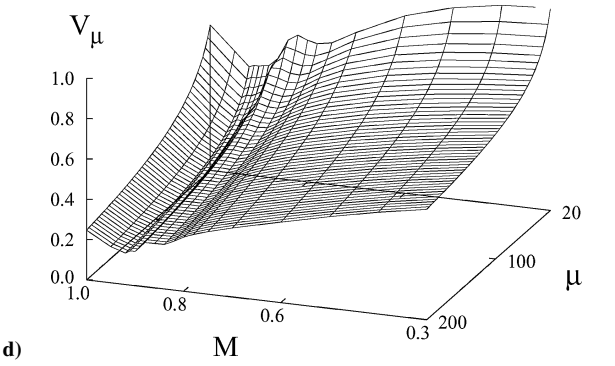

d)

Fig. 5 Static unbalance effect; flutter speed index vs Mach number and mass ratio: a) $x_\alpha = 0.00$, b) $x_\alpha = 0.10$, c) $x_\alpha = 0.25$, and d) $x_\alpha = 1.00$ (NACA 65A004, $\omega_h/\omega_\alpha = 0.8$, $r_\alpha^2 = 0.75$, $a = -0.6$).

These results indicate that the flutter speed index is sensitive to the ratio of uncoupled natural frequencies. For example, comparing Figs. 7a and 7b one can observe an overall decrease of V_μ as the values of ω_h/ω_α are increased from 0.5 to 0.8. Of course it is known[2] that the flutter speed index has a minimum near $\omega_h/\omega_\alpha = 1$. For a detailed discussion of the dependence of flutter results on the mass ratio and the ratio of uncoupled natural frequencies, the reader is referred to a recent work by the authors on this subject.[2]

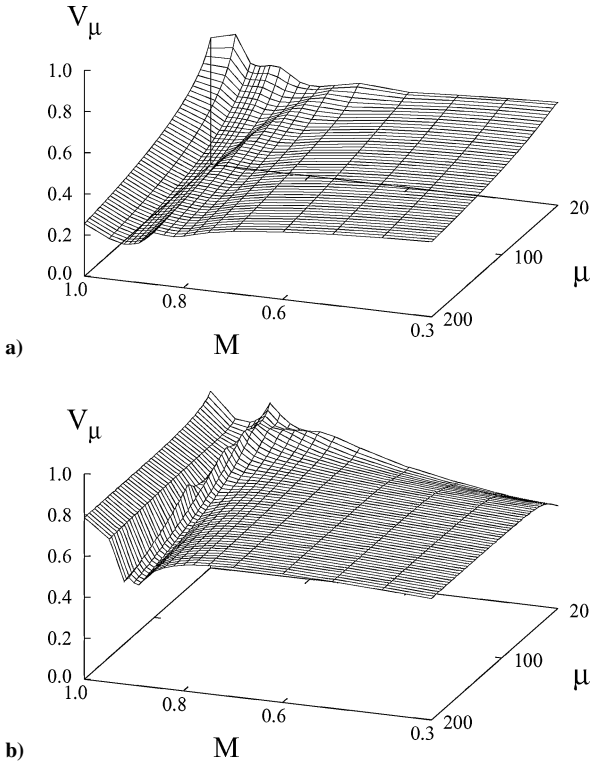

Fig. 6 Radius of gyration effect; flutter speed index vs Mach number and mass ratio: a) $r_\alpha^2 = 0.25$ and b) $r_\alpha^2 = 4.00$ (NACA 65A004, $\omega_h/\omega_\alpha = 0.8$, $x_\alpha = 0.25$, $a = -0.6$).

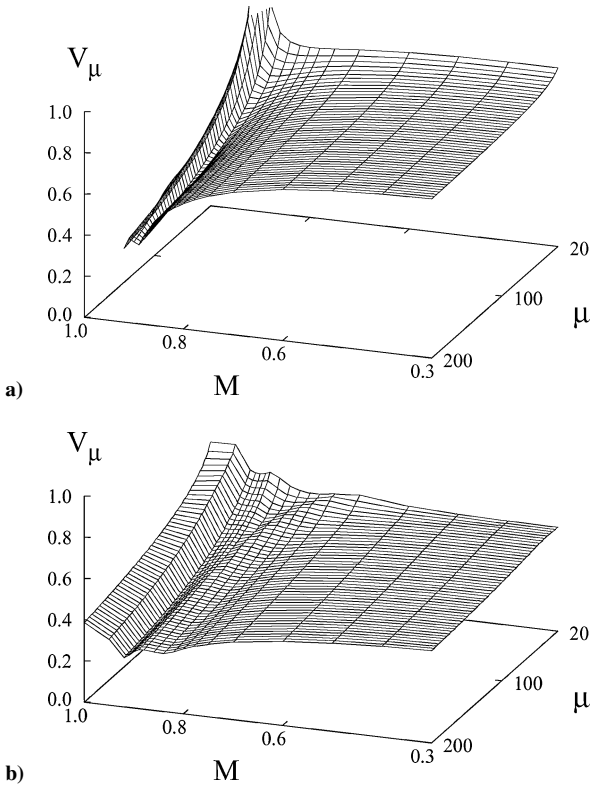

Fig. 7 Bending-torsion frequency ratio effect; flutter speed index vs Mach number and Mass ratio: a) $\omega_h/\omega_\alpha = 0.5$ and b) $\omega_h/\omega_\alpha = 0.8$ (NACA 65A004, $x_\alpha = 0.25$, $r_\alpha^2 = 0.75$, $a = -0.6$).

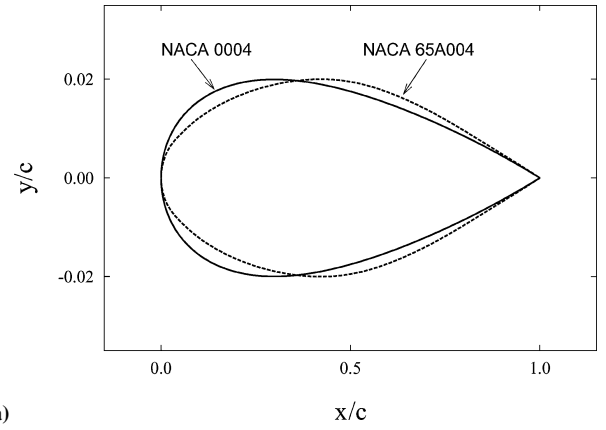

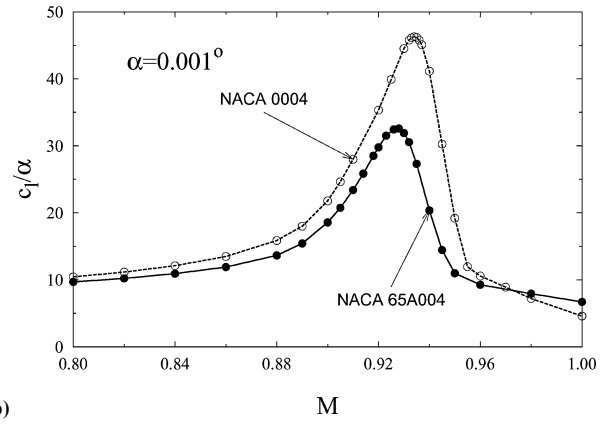

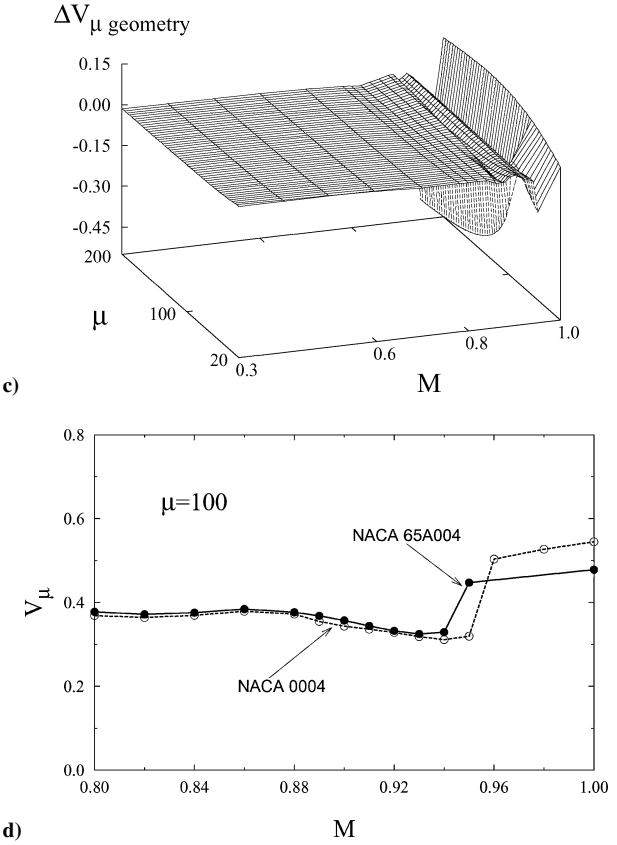

Fig. 8 Airfoil geometry effect for NACA 0004 and NACA 65A004 airfoils: a) airfoils geometry; b) ratio of steady lift to pitch angle vs Mach number; c) relative difference in flutter speed index, $\Delta V_{\mu_{\text{geometry}}} \equiv (V_{\mu_{\text{NACA0004}}} - V_{\mu_{\text{NACA65A004}}})/V_{\mu_{\text{NACA0004}}}$, vs Mach number and mass ratio; and d) flutter speed index vs Mach number at $\mu = 100$ ($x_\alpha = 0.25$, $r_\alpha^2 = 0.75$, $a = -0.6$, $\omega_h/\omega_\alpha = 0.8$).

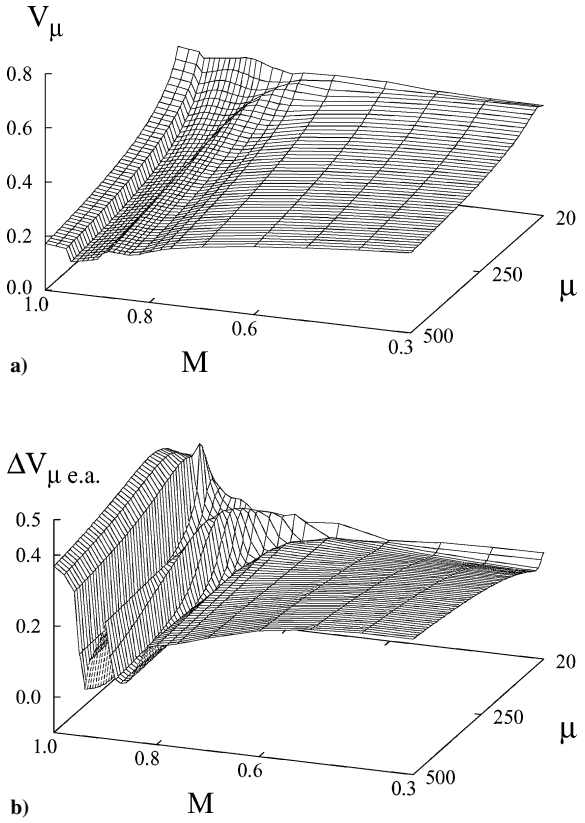

Fig. 9 Location of elastic axis effect: a) flutter speed index vs Mach number and mass ratio for $a = 0.0$; b) relative difference in flutter speed index, $\Delta V_{\mu_{ea}} \equiv (V_{\mu_{a=-0.6}} - V_{\mu_{a=0}})/V_{\mu_{a=-0.6}}$, vs Mach number and mass ratio (NACA 0004, $x_\alpha = 0.25$, $r_\alpha^2 = 0.75$, $\omega_h/\omega_\alpha = 0.8$).

Airfoil Geometry Effect

Dependence of the flutter speed index on the geometry of airfoil is shown for NACA 0004 and NACA 65A004 airfoils in Fig. 8. Both airfoils have 4% thickness-to-chord ratio but belong to two different families of NACA airfoils. One of the main differences in the geometry of these airfoils is the location of the point of maximum thickness. This point is shifted aft for the NACA 65A004 airfoil compared to the NACA 0004 airfoil (see Fig. 8a). Figure 8b shows the lift curve slope coefficients for these two airfoils. Note that the peaks in Fig. 8b occur in the range $0.92 < M < 0.94$. The relative difference in flutter speed index of these airfoils is shown in Fig. 8c. Note that this difference is the most dramatic (up to 45% at some mass ratios) at Mach number $M = 0.95$, that is, at a Mach number higher than those where the peaks in the lift curve slope coefficients occur. This can be seen better in Fig. 8d.

Location of Elastic Axis Effect

Dependence of the flutter speed index on the location of elastic axis, $a = e/b$, is shown in Fig. 9. The elastic axis for the NACA 0004 airfoil was placed at one-fifth, $a = -0.6$, and also the middle, $a = 0.0$, of the chord. The flutter speed index for the case of midchord elastic axis location is shown in Fig. 9a. (The respective result for $a = -0.6$ was shown earlier in Fig. 3a.) The relative difference in flutter speed index for the two cases is shown in Fig. 9b. The results indicate that moving the elastic axis aft from $a = -0.6$ to $a = 0.0$ decreases the flutter speed index in subsonic Mach numbers by 30%. The largest difference (approximately 50%) in the flutter speed index occurs at Mach numbers close to $M = 1$.

Conclusions

In this paper, the advantages of presenting the transonic flutter velocity as a function of the Mach number and mass ratio in a three-parameter map are demonstrated. This is particularly useful for simulating a wind-tunnel flutter trajectory or doing a flutter parameter study. For example, in the case of comparing computational results with experimental data such a map provides a much clearer understanding of where an experimental system flutters at a given speed of sound and Mach number. Numerical results generally agreed well with the experiment.

Flutter similarity for airfoils of different thickness was considered to test recent developments on this subject.[7] Equivalent transonic flutter parameters for NACA 0004 and NACA 0012 airfoils agreed well except for (equivalent) Mach numbers above the transonic dip.

References

[1]Bendiksen, O. O., "Transonic Flutter and the Nature of the Transonic Dip," *Proceedings of the CEAS/AIAA/AIAE International Forum on Aeroelasticity and Structural Dynamics*, Vol. 2, Madrid, Spain, June 2001, pp. 273–286.

[2]Kholodar, D. B., Thomas, J. P., Dowell, E. H., and Hall, K. C., "A Parametric Study for an Airfoil in Inviscid Transonic Flow," *Journal of Aircraft*, Vol. 40, No. 2, 2003, pp. 303–313.

[3]Dowell, E. H., and Tang, T., "Nonlinear Aeroelasticity and Unsteady Aerodynamics," *AIAA Journal*, Vol. 40, No. 9, 2002, pp. 1697–1007.

[4]Dowell, E. H., and Hall, K. C., "Modeling of Fluid-Structure Interaction," *Annual Review of Fluid Mechanics*, Vol. 33, 2001, pp. 445–490.

[5]Hall, K. C., Thomas, J. P., and Clark, W. S., "Computation of Unsteady Nonlinear Flows in Cascades Using a Harmonic Balance Technique," *AIAA Journal*, Vol. 40, No. 5, 2002, pp. 879–886.

[6]Rivera, J. A., Dansberry, B. E., Bennett, R. M., Durham, M. H., and Silva, W. A., "NACA 0012 Benchmark Model Experimental Flutter Results with Unsteady Pressure Distributions," NASA TM 107581, March 1992.

[7]Bendiksen, O. O., "Improved Similarity Rules for Transonic Flutter," AIAA Paper 99-1350, April 1999.

[8]Spreiter, J. R., "On the Application of Transonic Similarity Rules to Wings of Finite Span," NACA Rept. 1153, 1953.

[9]Spreiter, J. R., "On Alternative Forms for the Basic Equations of Transonic Flow Theory," *Journal of the Aeronautical Sciences*, Vol. 21, Jan. 1954, pp. 70–72.